Supporting Information

Molecular Dynamics Simulation of DNA Capture and Transport in Heated Nanopores

Maxim Belkin and Aleksei Aksimentiev[*]

Department of Physics, University of Illinois at Urbana-Champaign

E-mail: aksiment@illinois.edu

[*]To whom correspondence should be addressed

General MD Protocols

All MD simulations reported in this study were performed using the program NAMD2.[1] The interatomic interactions were described by the CHARMM27[2] force field employing the Lorentz-Berthelot combining rules for interactions between non-bonded atoms and TIP3P water model. CHARMM-compatible parameters for silicon oxide[3] were used in the simulations of plasmonic nanopores. The Lennard-Jones parameters for atoms of gold were: ε = -0.039 kcal/mol and $R_{min}/2$ = 1.0368 Å.[4] NBFIX corrections to the Lennard-Jones parameters were applied for specific ion pairs as reported in ref. 5. All simulations employed periodic boundary conditions, 2–2–6 fs multiple timestepping, SETTLE algorithm to keep water molecules rigid,[6] RATTLE algorithm to keep rigid all other covalent bonds involving hydrogen atoms,[7] a 7–8 Å cutoff for van der Waals and short-range electrostatic forces, and the particle mesh Ewald (PME) method[8] over a 1.0 Å resolution grid for long-range electrostatic interactions.
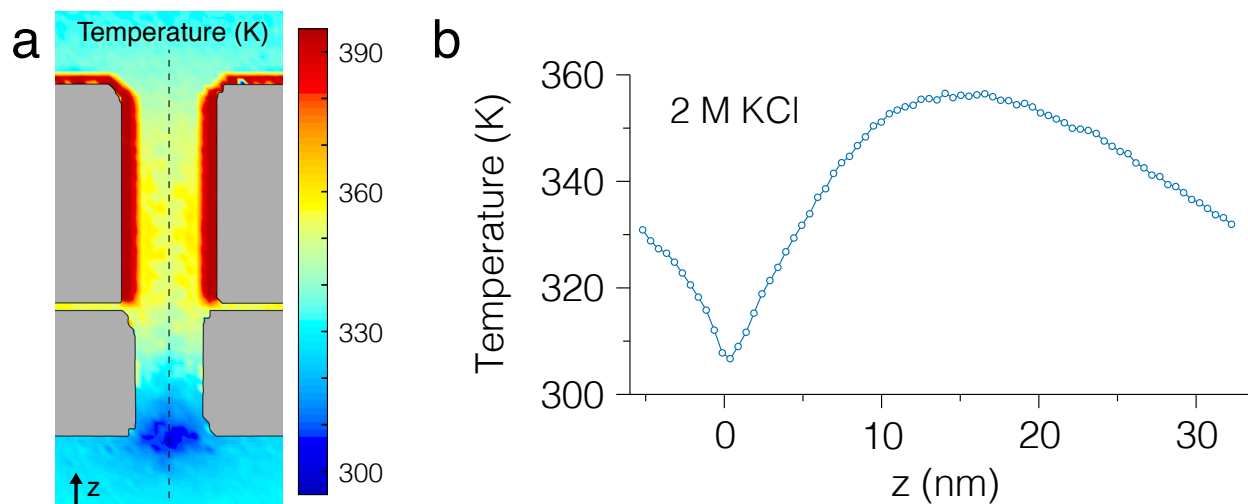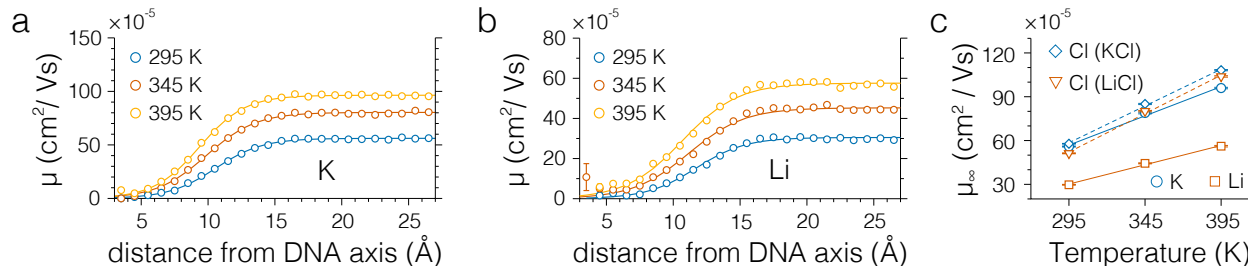

Supplementary Figure S1. **Distribution of temperature in all-atom MD simulations of locally-heated plasmonic nanopores.** (a) Local temperature map of the simulated plasmonic nanopore system. In these simulations the bow tie temperature is set to 395 K whereas the temperature of a 5 Å-thick slab of water at the opposite side of the membrane is set to 295 K. The cooled water slab is parallel to the membrane. Regions of the system devoid of atoms (interior volumes of the membrane and bow tie) are shown in grey. The dashed line indicates the center axis of the plasmonic nanopore. (b) 1-D temperature profile sampled along the central axis of the plasmonic nanopore (defined in panel a).

Simulations of DNA Capture and Translocation

For simulations of DNA capture in a heated nanopore, we built an all-atom system that featured a 10 nm-thick SiO_2 membrane with a nanopore, plasmonic gold bow tie nanoantenna residing on top of the pore, and a short 20-bp piece of dsDNA, Figure 1 b. The membrane was built using the **INORGANIC BUILDER** plugin of VMD[9] following the procedures described elsewhere.[10] A nanopore of an hourglass shape with the inner and outer diameters of 3.5 and 5 nm, correspondingly, was cut from the membrane by removing atoms that satisfied the mathematical condition of the shape. We also removed atoms of the membrane that were more than 0.3 nm away from the surface, which made the membrane effectively hollow but still impermeable to water, ions, and DNA. By doing
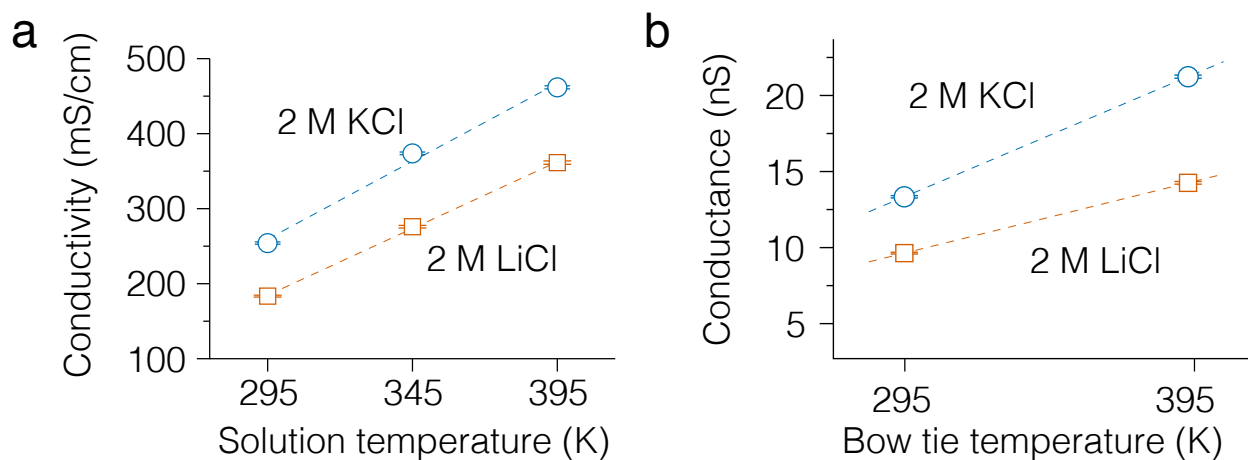
Supplementary Figure S2. **Simulated temperature dependence of bulk electrolyte conductivity and open pore conductance.** (a) Conductivity σ of 2 M KCl and 2 M LiCl bulk electrolyte solutions as a function of temperature in all-atom MD simulations. The conductivity values were extracted from the simulations of DNA in a bulk solution as j_0/E, where j_0 was the total ionic current density in the bulk region (further that 22.5 Å from the DNA central axis) and E was the magnitude of the applied electric field corresponding to a potential drop of 350 mV over 10 nm distance. The simulation system used for these calculations is shown in Figure 3 a. The simulated relative increase of bulk conductivity $(\sigma_{395K} - \sigma_{295K})/\sigma_{295K}$ was 82% for KCl and 97% for LiCl. (b) The simulated conductance G of a solid-state plasmonic nanopore (Figure 1 b) in the absence of DNA for 2 M KCl and 2 M LiCl solutions as a function of the bow tie temperature. Dashed lines show linear fits to the data. The simulated relative increase of the nanopore conductance $(G_{395K} - G_{295K})/G_{295K}$ was 59% and 48% for the KCl and LiCl solution, respectively. The temperature dependence of the open pore conductance does not follow the temperature dependence of the bulk electrolyte conductivity because the temperature of the solution in the nanopore volume is considerably lower than the temperature of the bow tie, Figure S1.

Supplementary Figure S3. **Simulated dependence of ion mobility on the distance from DNA and temperature.** (a–b) Radial profiles of cation mobility as a function of the distance from the DNA axis in MD simulations of the DNA system shown in Figure 3 a. Data in panels a and b were obtained for 2 M KCl and 2 M LiCl electrolyte solutions, respectively. (c) Temperature dependence of the ion mobility in the bulk electrolyte region of the simulate system. Each data point was obtained by averaging the radial mobility profiles (panels a and b) over the region located more than 22 Å away from the DNA axis.

so, we significantly reduced the total number of atoms in the system while preserving description of specific interactions between DNA and the membrane. The remaining membrane atoms were then annealed[3] applying a grid potential[11] to maintain the prescribed shape. In all production simulations of DNA capture and translocation, all SiO_2 atoms were harmonically restrained to the coordinates attained at the end of the annealing simulation.

The tips of the bow tie nanoantenna were cut from a ~ 20 nm-thick gold membrane prepared using the **INORGANIC BUILDER** plugin of VMD. The shape of the tips was chosen to reproduce the experimental curvature of gold nano-triangles.[12] As with the membrane, gold atoms that were more that 0.3 nm away from the surface of the bow tie were removed. The annealing procedure was not applied to the gold atoms. In all production simulations, the gold atoms were harmonically restrained to their initial coordinates.

A short 20-bp piece of a double stranded DNA molecule was prepared using the 3D-DART server.[13] One strand of the molecule had the sequence: 5′-GACTATCTGCCCGTCTACTC-3′. The molecule was placed concentrically with the nanopore (z) axis ~ 10 nm above the pore entrance. A set of harmonic constraints applied to the phosphorus atoms of the DNA *via* the **TCLFORCES** feature of NAMD, restricting the motion of the molecule to translation along the z-axis and rotation about that axis. The use of such constraints prevented non-specific interactions between DNA and
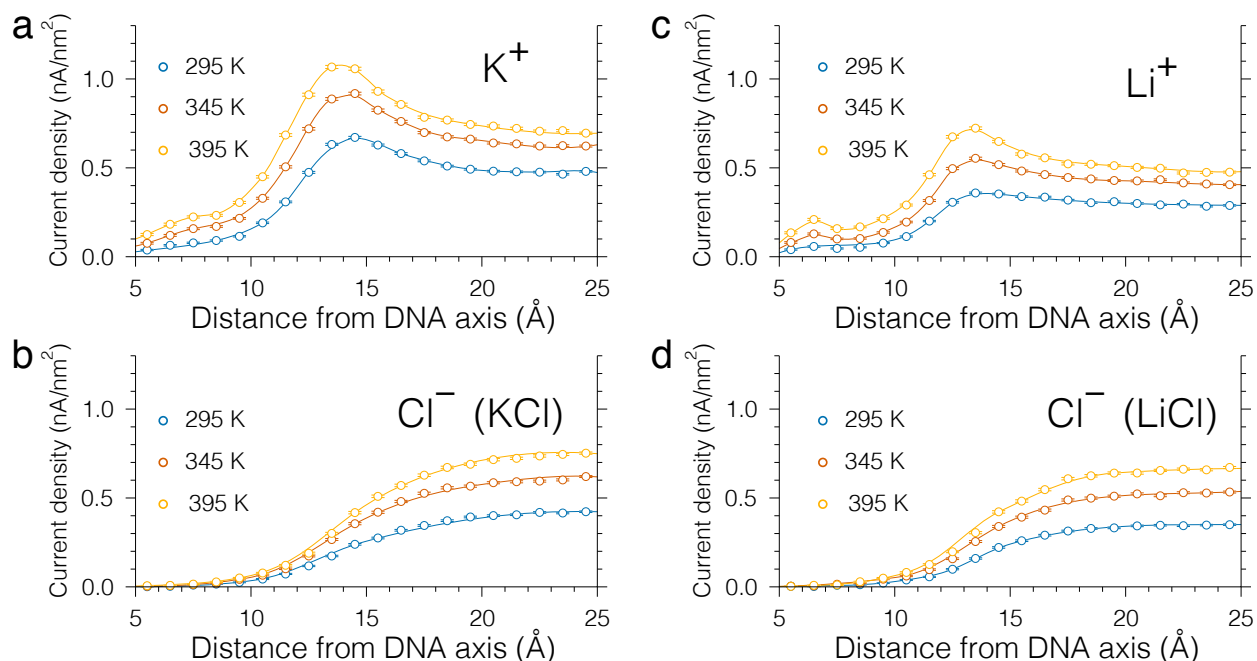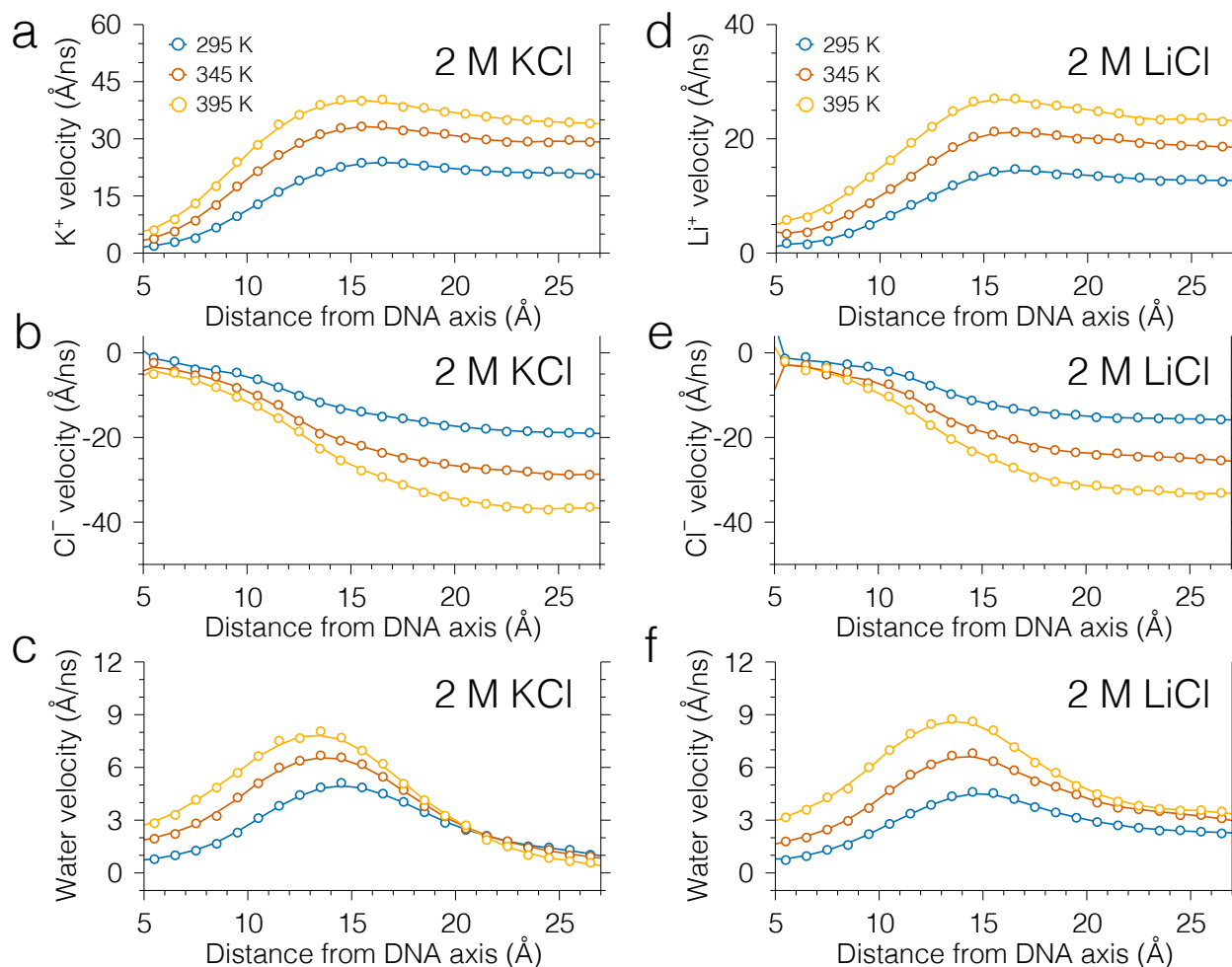
Supplementary Figure S4. **Ionic current density as a function of the distance from the DNA axis** in (a–b) 2 M KCl, and (c–d) 2 M LiCl. A typical simulation system used for these calculations is shown in Figure 3 a. To compute the current density profiles, the volume around the DNA molecule was partitioned into 1 Å-wide radial bins centered on the DNA axis. The bin size L_z along the DNA axis was 6 nm; the bins were centered on the midplane of the helix. The ionic current in each bin was computed as $I = \sum_{i,t} q_i \Delta z_i / L_z T$, where q_i and Δz_i were the charge and displacement of ions along the z axis in the bin, T was the total simulation time, and summation $\sum_{i,t}$ was performed over all ions that populated the bin and over all frames of the MD trajectory. The current density profiles were then obtained by dividing the total average current in each bin by the cross-sectional (xy) area of the bin.

the solid-state membrane, singling out the effects of electrolyte composition and localized heating on DNA capture and translocation process. Hydrogen bonds within the basepairs of the molecule were enforced using the **EXTRABONDS** feature of NAMD. The equilibrium lengths of the hydrogen bonds for the **EXTRABONDS** restraints were determined from the simulations of DNA where such retratins were not applied.

A system containing the solid-state membrane, the gold bow tie nanoantenna, and the DNA molecule was solvated using the **SOLVATE** plugin of VMD, producing a $\sim 13 \times 18 \times 38.5$ nm^3 system, ~ 0.52 million atoms in total. Ions were then added to the system using the **AUTOIONIZE** plugin of VMD in the amounts necessary to produce neutral 2 M KCl and 2 M LiCl solutions.

Following assembly, each system underwent 1,200 steps of energy minimization using the conjugate gradient method followed by $\sim 500{,}000$ steps (~ 1 ns) of equilibration in the NPT ensemble (constant number of particles N, pressure P, and temperature T). During equilibration a
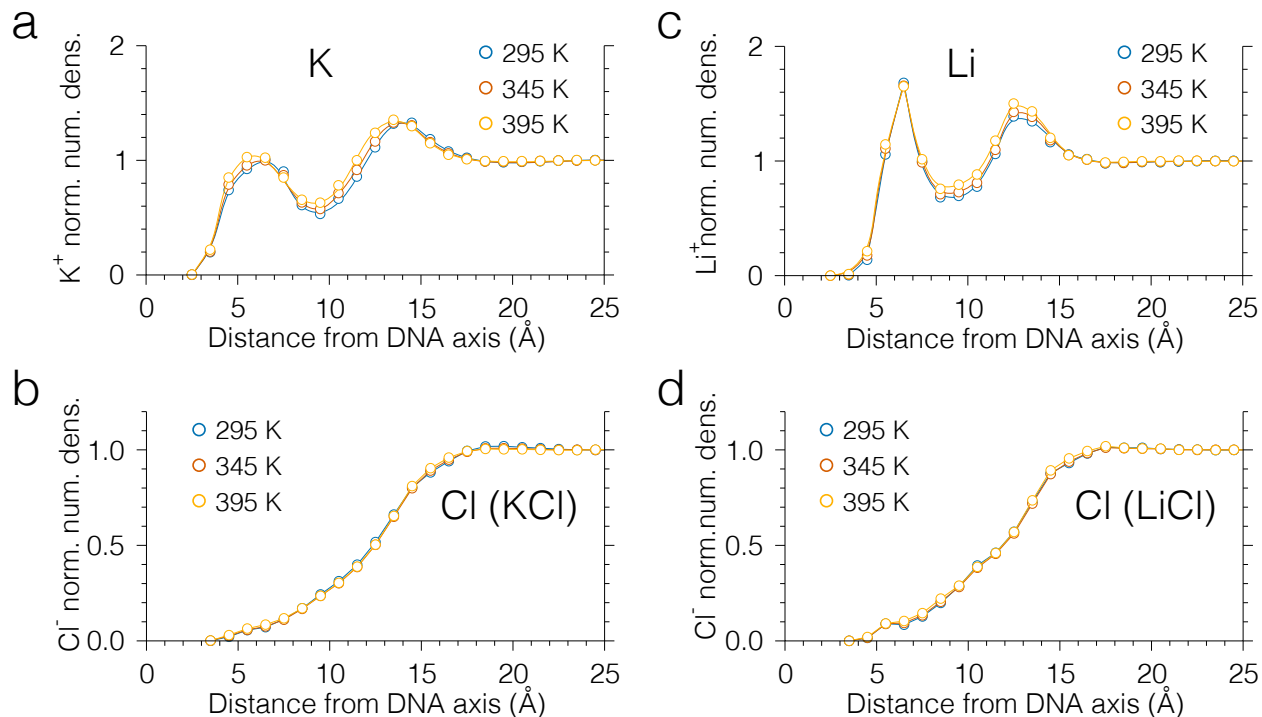

Supplementary Figure S5. **Radial profiles of ion and water velocities near DNA.** (a–c) The average z-component of potassium (panel a), chloride (panel b) and water (panel c) velocities in MD simulations of DNA in 2 M KCl solution as a function of the distance from the DNA axis. (d–f) The average z-component of lithium (panel d), chloride (panel c) and water (panel f) velocities in MD simulations of DNA in 2 M LiCl solution as a function of the distance from the DNA axis. A typical simulation system used for these calculations is shown in Figure 3 a; the applied electric field was 35 mV/nm directed along the z axis. The following three temperatures of the bulk solutions were investigated: 295, 345 and 395 K. To compute the velocity profiles, the volume around the DNA molecule was partitioned into 1 Å-wide radial bins centered on the DNA axis. Along the DNA axis, the bin size was 6 nm; the bins were centered on the midplane of the helix. The average velocity in each bin was determined by averaging over all particles present in the respective bins and over all frames of the respective MD trajectory.

Lowe-Andersen[14] thermostat kept the temperature at 295 K, Nosé-Hoover Langevin piston pressure control[15] maintained the pressure at 1 atm by adjusting the system's dimension along the z axis.

Two sets of production simulations were performed for each electrolyte solution. In the first set, the entire system was maintained at a uniform temperature of $T_{eq} = 295$ K. In the second set, the temperature of the gold bow tie was maintained at $T_{bt} = 395$ K by coupling its atoms to a Langevin thermostat. Another, local Lowe-Andersen thermostat was activated in a 0.5 nm-thick slab perpendicular to the z axis and was coupled to the water molecules only. A detailed description of the implementation and application of such local thermostats with NAMD2 can be found in our previous publications.[16,17] In all simulations, a uniform electric field was applied normal to the membrane producing a 350 mV voltage bias across the simulation system.[18,19]

Simulations of the Effective Force in a Heated Nanopore

To measure the effective force of the electric field on dsDNA in a heated nanopore, we combined the previously described all-atom model of the solid-state membrane and the bow tie with a 77-basepair dsDNA and each of the following three electrolyte solutions: 1 M KCl, 2 M KCl, and 2 M LiCl, Figure 4 a. Using a custom **TCLFORCES** script, each phosphorus atom of the DNA molecule was restrained to remain at the surface of a virtual cylinder with a diameter of 2 nm *via* a harmonic force acting within the $x - y$ plane only; the spring constant of each harmonic restraint was $k_r = 100$ pN/Å. The script also harmonically restrained the CoM of all phosphorus atoms along the vertical z axis to its initial location with a spring constant of $k_z = 152$ pN/Å. The restraining forces and the CoM coordinates were updated every 500 steps, or 1 ps. A transmembrane bias of 350 mV was applied across the system normal to the membrane. Similarly to our simulations of DNA capture, two sets of simulations were performed for each electrolyte type: one at a uniform temperature of 295 K and the other reproducing the local heating of the bow tie. Each system was simulated for 50 ns. The water flow reached a steady state within the first 10 ns. For each condition, the effective force was computed by averaging over the last 40 ns of the simulation trajectory.

Supplementary Figure S6. **Simulated dependence of normalized ion number density on the distance from DNA and temperature.** Radial profiles of number densities of K^+ (panel a), Cl^- in KCl solution (panel b), Li^+ (panel c), and Cl^- in LiCl solution (panel d) are shown as functions of the distance from the DNA axis. The profiles are normalized by the corresponding average ion number density in the bulk region of the system (farther than 22 Å from the DNA axis). A typical simulation system used for these calculations is shown in Figure 3 a; the applied electric field was 35 mV/nm directed along the z axis.

Simulations of DNA in Bulk Electrolytes

For our simulations of dsDNA in a uniformly heated bulk electrolytes, we used a 22-bp dsDNA molecule extracted from a longer DNA molecule described in the previous section. The sequence of nucleotides in one of the molecule's strands was: 5′-TCTGCCCGTCTACTCGACTATC-3′. The DNA molecule was solvated and neutralized by adding ions in the amounts necessary to produce 2 M KCl, 2 M LiCl, or 2 M NaCl solutions. All systems had a hexagonal cross-section in the xy plane with a side of 5.2 nm, and initial length along the z axis of ~ 10.5 nm. The systems underwent energy minimization for 600 steps and 1 ns equilibration in the NPT ensemble with the Nosé-Hoover Langevin piston pressure control set to one of the following three temperatures: 295, 345, and 395 K; the $x - y$ cross-section was the same in all systems. During these equilibration

simulations the phosphorus atoms of DNA were restrained within the *xy* plane to remain at the surface of a virtual cylinder with a diameter of 2 nm. Upon equilibration, the systems' dimensions along the *z* axis at 295, 345 and 395 K were: 10.7, 11.1, and 11.7 nm for 2 M KCl, 10.5, 10.9, and 11.5 nm for 2 M LiCl, and 10.4, 10.9, and 11.4 for 2 M NaCl.

In the production simulations, a homogeneous electric field parallel to the *z* axis was applied. The magnitude of the electric field was chosen such that the electric potential drop was 350 mV over 10 nm, similar to the potential drop in the plasmonic nanopore systems. To measure the effective force experienced by the DNA in solutions at different temperatures, all phosphorus atoms of
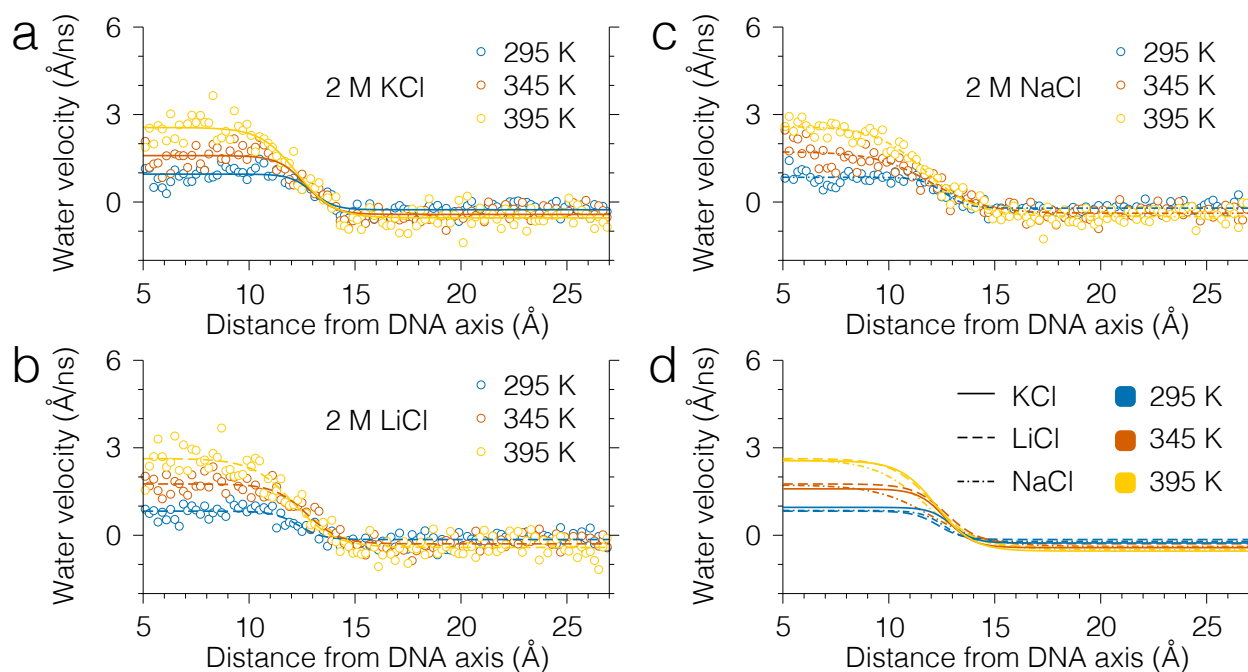
Supplementary Figure S7. **Radial profiles of water velocities near DNA in simulations with suppressed water flows.** (a–c) The average *z*-component of water velocity in 2 M solutions of KCl (panel a), LiCl (panel b) and NaCl (panel c) in MD simulations as a function of the distance from the DNA axis. Lines shows fits to data of the smooth-step function: $v_z = a - b \tanh\left(\frac{r-c}{d}\right)$. Unlike normalized mobility that changes from zero to unity, velocity values near the DNA and away from it are independent parameters. As a result, four fitting parameters are necessary to fit the location and width of the smooth step (parameters *c* and *d*) as well as velocity values near the molecule and away from it (parameters *a* and *b*) independently. (d) The fits of a smooth-step function to data from panels (a–c). The fits show that water velocity profiles at a given temperature are almost identical in all three solutions and the difference does not exceed 0.5 Å/ns. Decay of water velocity is only slightly smoother in NaCl than in the other two solutions at 345 and 395 K.

the molecule were harmonically restrained to their initial coordinates in all three spatial directions with a spring constant of $k_{bulk} = 10$ pN/Å. The restraining forces were recorded every 50 steps, or 0.1 ps. Each system was simulated for 500 ns. Additional 220 ns-long simulations were performed for each system under the water flow canceling protocol (described below in the **Suppression of Water Flow near DNA** section).

Calculation of Ion Mobility near DNA

Simulations of DNA in bulk electrolyte solutions under a uniform electric field (see previous section) were used to compute radial distributions of ion mobility. The position-dependent mobility was calculated as[20] $\mu = (v - u)/E$, where v and u were the velocities of the ions and water, correspondingly, parallel to the applied electric field $\vec{E} = E\vec{z}$. The instantaneous velocities of the ions and water molecules were averaged in concentric cylindrical shell bins that were defined as: $r_{n,min} \leq r < r_{n,max}$, where $r = \sqrt{x^2 + y^2}$ was the radial coordinate of an ion or a water molecule in the $x - y$ plane, $r_{n,min} = 0.3 \cdot n$ (nm) and $r_{n,max} = r_{n,min} + 0.3$ (nm) were the minimum and maximum radii of the n-th shell bin.

Suppression of Water Flow near DNA

A proportional-integral-derivative (PID) control mechanism was used to suppress the water flows in simulations of DNA in bulk electrolyte. The PID controller was realized as a custom Tcl script engaged by NAMD *via* its TCLFORCES feature. The controller virtually divided the space around the molecule into concentric cylindrical shells aligned with the molecule's axis and computed mean water velocity in each of them every 1 ps. The outer radius of each cylindrical shell exceeded the inner one by 0.3 nm. The cylindrical shell closest to the molecule had the inner diameter of 1.25 nm so that binding of ions to the DNA remained unaffected. The length of all shells along the molecule's axis was 6 nm and, therefore, did not exceed the length of the molecule.

Mean water velocity in the cylindrical shells was used to compute the three components of the force applied by the PID controller. The proportional term was computed as $F_P = \gamma \left(v_{target} - v_{water} \right) =$

$-\gamma v_{\text{water}}$, where v_{water} is the mean water velocity in a shell measured in Å/ps, $v_{\text{target}} \equiv 0$ Å/ps is the target velocity, and coefficient γ was set to $0.01 \frac{\text{kcal}}{\text{mol}\,\text{Å}} / \frac{\text{Å}}{\text{ps}}$. With such a coefficient, the PID controller applied a force of 0.69 pN along the molecule's axis to those water molecules that moved along that axis at a speed of 1 Å/ps. The value of γ was chosen such that the proportional term of the controller on its own provided significant flow compensation. Larger values of γ led to occasional termination of simulations caused by high forces applied by the controller to water molecules and, therefore, were avoided.

Computed mean water velocities in virtual cylindrical shells were recorded and used for the calculation of the integral term of the controller as $F_{\text{I}} = \xi \frac{1}{N_{\text{rec}}} \sum_{i}^{N_{\text{rec}}} \left(v_{\text{target}} - v_{\text{water},\, i} \right) = -\xi \frac{1}{N_{\text{rec}}} \sum_{i}^{N_{\text{rec}}} v_{\text{water},\, i}$, where N_{rec} is the number of historical records of the water velocity in a cylindrical shell, $v_{\text{water},\, i}$ is the i-th value of average water velocity in that shell (i runs from 1 to N_{rec}), $v_{\text{target}} \equiv 0$ Å/ps is the target velocity for all shells, and coefficient ξ was set to $0.025 \frac{\text{kcal}}{\text{mol}\,\text{Å}} / \frac{\text{Å}}{\text{ps}}$. The value of ξ was chosen to provide optimal flow compensation. The derivative term of the controller was not engaged in production simulations because of the high variability of the 1 ps-averaged velocity measurements.

Simulations of the Relative Bulk Solution Viscosities

To elucidate the dependence of the electrolytes' viscosity on temperature and ion composition, we simulated a cubic volume (~ 5 nm on each side) of 2 M KCl and 2 M LiCl electrolyte solutions at uniform temperature of 295, 345, or 395 K. In these simulations, a steered MD (**SMD**) feature of NAMD was employed to pull a single water molecule along the z axis with a constant velocity $v_{\text{pull}} = 10$ nm/ns, Figure 4 f. The spring constant used in the constant velocity pulling SMD protocol was set to 100 pN/Å; no restraints were applied within the plane perpendicular to the direction of pulling (the $x - y$ plane in our simulations). The force F_{pull} required to maintain the pulling velocity was recorded every 0.96 ps. To prevent the system from drifting in the direction of the pulling, the CoM of the remaining atoms was harmonically restrainted to its initial position *via* a harmonic spring ($k_{\text{spring}} = 100$ pN/Å) using a custom **TCLFORCES** script. In the regime of low pulling velocities, the pulling force exactly compensates the Stokes' viscous drag: $\vec{F}_{\text{pull}} = -\vec{F}_{\text{drag}}$,

which, according to the Stokes equation, is proportional to the product of the pulling velocity $\vec{v}_{\text{pull}}$ and the solution viscosity η. Alternatively, one can write $\eta \sim F_{\text{pull}}/v_{\text{pull}}$. Choosing the viscosity of 2 M KCl solution at 295 K, $\eta_{\text{KCl}}(295 \text{ K})$, as a reference, we characterized the viscosity at all other electrolyte and temperature conditions by the ratio of the average pulling forces, Figure 4 g.

Calculation of Ion Residence Time near DNA

To compute the average residence time of ions near the DNA molecule, we used the method previously described in ref. 21. First, we selected all water molecules located within 3.1 Å of the non-hydrogen atoms of the DNA. Next, we selected all cations and anions located closer than 3.4 Å (cations) or 3.7 Å (anions) from the selected water molecules. Following that, we compute the lifetime of each specific water-ion pair using MD trajectories sampled every $\Delta t = 9.6$ ps. The lifetime of a water-ion pair was defined as the product of Δt and $(N - 1)$, where N was the number of consecutive frames the specific pair remained present according to the above selection procedure. Because of thermal fluctuations, the absolute ion binding times determined using the above method can depend on the sampling frequency of the MD trajectory. Nevertheless, the relative changes of the ion binding time with temperature and ion type are independent of the trajectory sampling frequency.

Conductance Blockades as a Function of Ion Mobility

Electrophoretic transport of a charged molecule such as DNA through a nanopore in a membrane is accompanied by the suppression of the flow of ions that compete with the molecule for the nanopore volume. This suppression of the ionic current is typically characterized by absolute and relative conductance blockades. The absolute conductance blockade is defined as:

$$\Delta G = \frac{\Delta I}{V_{\text{t}}} = \frac{I_{\text{b}} - I_0}{V_{\text{t}}}, \tag{1}$$

where I_b and I_0 are the blockade and open pore currents, correspondingly, and V_t is the applied transmembrane bias.

For a flow of ions in a bulk solution, the above formula has to be reformulated. We start by noting that ionic current I can be written in the form of an integral of the current density over the system's volume:

$$I = \int_0^{2\pi} d\phi \int_0^{\infty} q\, n(r)\, v(r)\, r\, dr, \tag{2}$$

where ϕ and $r = \sqrt{x^2 + y^2}$ are the azimuth and radial distance in a cylindrical coordinate system, q, n, and v are the charge, number density and velocity of ions. Using Equation 2, we can rewrite the current reduction ΔI as:

$$\Delta I = I_b - I_0 = \sum \int_0^{2\pi} d\phi \int_0^{\infty} q\left(n(r)v(r) - n_\infty v_\infty\right) r\, dr, \tag{3}$$

where the summation is performed over different ion types in the solution (e.g. K^+, Li^+, Cl^-). Noting that integration over ϕ yields a scaling factor of 2π and that $V_t = EL_z$, where E is the electric field magnitude and L_z is the dimension of the simulation system in the direction of the applied field, we can rewrite Equation 1 as follows:

$$\Delta G = \frac{I_b - I_0}{EL_z} = \frac{2\pi}{L_z} \sum q \int_0^{\infty} \left(n(r)\frac{v(r)}{E} - n_\infty \frac{v_\infty}{E}\right) r\, dr, \tag{4}$$

where $v/E = \mu$ is the ion mobility. Away from the DNA, the ion number density $n(r)$ and the ion velocity $v(r)$ return to their bulk solution values n_∞ and v_∞. We define distance R_* such that:

$$n(r \geq R_*) = n_\infty$$
$$v(r \geq R_*) = v_\infty. \tag{5}$$

For a DNA molecule in a bulk electrolyte, $R_* = 2.2$ nm, see Figures S4 and S7. Integration over

radial distance can be split into two regions $\int_0^\infty = \int_0^{R_*} + \int_{R_*}^\infty$. Clearly, integration over the second region ($R_* \to \infty$) yields 0, so we arrive at:

$$\Delta G = \frac{2\pi}{L_z} \sum q \int_0^{R_*} \left(n(r)\mu(r) - n_\infty\mu_\infty \right) r\,dr$$

$$= \frac{2\pi}{L_z} \sum q\mu_\infty n_\infty \int_0^{R_*} \left(\frac{n(r)}{n_\infty} \frac{\mu(r)}{\mu_\infty} - 1 \right) r\,dr$$

$$= \frac{2\pi}{L_z} \sum q\mu_\infty n_\infty \int_0^{R_*} \left(n^*(r)\mu^*(r) - 1 \right) r\,dr \tag{6}$$

where $\mu^* = \mu/\mu_\infty$ and $n^* = n/n_\infty$ are the normalized mobility (main text Figure 3 d–e) and the normalized number density, Figure S6, correspondingly. For 1:1 electrolyte solutions, the number densities of the charge carriers in the bulk regions (n_∞) are identical and can be moved outside the summation. From Equation 6, one can immediately notice that temperature dependence of the absolute conductance blockade comes from the variation of the ion mobility in the bulk solution μ_∞, which, unlike the number density n_∞, does depend on the solution temperature, and the integral $\int_0^{R_*} \left(n^*(r)\mu^*(r) - 1 \right) r\,dr$. Note that the magnitude of the conductance blockade does not depend on the precise value of R_* as long conditions of Equations 5 are met. The absolute conductance blockades computed using Equation 6 are shown in main text Figure 3 f.

The relative conductance blockade of a nanopore is defined as:

$$\frac{\Delta G}{G} = \frac{\Delta I}{I_0} = \frac{I_b - I_0}{I_0}. \tag{7}$$

The relative blockade clearly depends on the absolute value of the nanopore conductance and, therefore, on the physical dimensions of the nanopore. To elucidate the temperature dependence

of the relative conductance blockade, let's rewrite Equation 7 as:

$$\frac{\Delta G}{G} = \frac{2\pi \sum q \int (n(r)\mu(r) - n_\infty\mu_\infty)\, rdr}{2\pi \sum q \int n_\infty\mu_\infty rdr} = \frac{\sum q n_\infty\mu_\infty \int (n^*(r)\mu^*(r) - 1)\, rdr}{\sum q n_\infty\mu_\infty \int rdr}, \qquad (8)$$

where we purposefully omitted the integration limits as they require special consideration. The expression inside the integral in the numerator is 0 for $r > R_*$, hence the integration can be limited to a region where the mobility and the number density of ions deviate from their bulk values, *i.e.* $r \in [0; R_*)$. In the denominator, however, integration beyond R_* does not yield zero so the upper integration limit (R_0) must be explicitly set. To enable comparison to the results of direct ionic current calculations, Figure 3 c, we set R_0 to 2.7 nm. Finally, we can write the expression for the relative conductance blockade as:

$$\frac{\Delta G}{G} = \frac{\sum q n_\infty\mu_\infty \int_0^{R_*} (n^*(r)\mu^*(r) - 1)\, rdr}{\sum q n_\infty\mu_\infty \int_0^{R_0} rdr} = \frac{\sum q n_\infty\mu_\infty \int_0^{R_*} (n^*(r)\mu^*(r) - 1)\, rdr}{\sum q n_\infty\mu_\infty \dfrac{R_0^2}{2}} \qquad (9)$$

The relative conductance blockades computed using Equation 9 are shown in main text Figure 3 g. The above equation demonstrates that the relative blockade depends not only on the mobility of ions in the bulk solution (μ_∞) but also on the dependence of ionic mobility on the distance from the DNA. Equation 9 allows us to model a situation when the normalized ion mobility does not depend on temperature of the solution. For this purpose, we calculate $\Delta G/G$ using Equation 9 but, instead of using the actual normalized mobility profiles, we use the profiles obtained in the simulations at 295 K. The relative conductance blockades obtained under such assumptions are shown in Figure 3 g (filled symbols).

References

(1) Phillips, J. C.; Braun, R.; Wang, W.; Gumbart, J.; Tajkhorshid, E.; Villa, E.; Chipot, C.; Skeel, R. D.; Kale, L.; Schulten, K. Scalable Molecular Dynamics with NAMD. *J. Comput. Chem.* **2005**, *26*, 1781–1802.

(2) Foloppe, N.; MacKerell Jr., A. D. All-Atom Empirical Force Field for Nucleic Acids: I. Parameter Optimization Based on Small Molecule and Condensed Phase Macromolecular Target Data. *J. Comput. Chem.* **2000**, *21*, 86–104.

(3) Cruz-Chu, E. R.; Aksimentiev, A.; Schulten, K. Water-Silica Force Field for Simulating Nanodevices. *J. Phys. Chem. B* **2006**, *110*, 21497–21508.

(4) Braun, R.; Sarikaya, M.; Schulten, K. Genetically Engineered Gold-Binding Polypeptides: Structure Prediction and Molecular Dynamics. *J. Biomater. Sci., Polym. Ed.* **2002**, *13*, 747–757.

(5) Yoo, J.; Aksimentiev, A. Improved Parametrization of Li^+, Na^+, K^+, and Mg^{2+} Ions for All-Atom Molecular Dynamics Simulations of Nucleic Acid Systems. *J. Phys. Chem. Lett.* **2012**, *3*, 45–50.

(6) Miyamoto, S.; Kollman, P. A. SETTLE: An Analytical Version of the SHAKE and RATTLE Algorithm for Rigid Water Molecules. *J. Comput. Chem.* **1992**, *13*, 952–962.

(7) Andersen, H. C. RATTLE: A "Velocity" Version of the SHAKE Algorithm for Molecular Dynamics Calculations. *J. Comput. Phys.* **1983**, *52*, 24–34.

(8) Batcho, P. F.; Case, D. A.; Schlick, T. Optimized Particle-Mesh Ewald/Multiple-Time Step Integration for Molecular Dynamics Simulations. *J. Chem. Phys.* **2001**, *115*, 4003–4018.

(9) Humphrey, W.; Dalke, A.; Schulten, K. VMD: Visual Molecular Dynamics. *J. Mol. Graphics* **1996**, *14*, 33–38.

(10) Comer, J.; Wells, D. B.; Aksimentiev, A. In *DNA Nanotechnology, Methods and Protocols*; Zuccheri, G., Samori, B., Eds.; Humana Press: New York, 2011; Vol. 749; Chapter 22, pp 317–358.

(11) Wells, D. B.; Abramkina, V.; Aksimentiev, A. Exploring Transmembrane Transport through α-Hemolysin with Grid-Steered Molecular Dynamics. *J. Chem. Phys.* **2007**, *127*, 125101.

(12) Nicoli, F.; Verschueren, D.; Klein, M.; Dekker, C.; Jonsson, M. P. DNA Translocations through Solid-State Plasmonic Nanopores. *Nano Lett.* **2014**, *14*, 6917–6925.

(13) van Dijk, M.; Bonvin, A. M. J. J. 3D-DART: A DNA Structure Modelling Server. *Nucleic Acids Res.* **2009**, *37*, W235–W239.

(14) Koopman, E. A.; Lowe, C. P. Advantages of a Lowe-Andersen Thermostat in Molecular Dynamics Simulations. *J. Chem. Phys.* **2006**, *124*, 204103.

(15) Martyna, G. J.; Tobias, D. J.; Klein, M. L. Constant Pressure Molecular Dynamics Algorithms. *J. Chem. Phys.* **1994**, *101*, 4177–4189.

(16) Belkin, M.; Maffeo, C.; Wells, D. B.; Aksimentiev, A. Stretching and Controlled Motion of Single-Stranded DNA in Locally Heated Solid-State Nanopores. *ACS Nano* **2013**, *7*, 6816–6824.

(17) Belkin, M.; Chao, S.-H.; Giannetti, G.; Aksimentiev, A. Modeling Thermophoretic Effects in Solid-State Nanopores. *J. Comput. Electron.* **2014**, *13*, 826–838.

(18) Aksimentiev, A.; Heng, J. B.; Timp, G.; Schulten, K. Microscopic Kinetics of DNA Translocation Through Synthetic Nanopores. *Biophys. J.* **2004**, *87*, 2086–2097.

(19) Aksimentiev, A.; Schulten, K. Imaging α-Hemolysin with Molecular Dynamics: Ionic Conductance, Osmotic Permeability and the Electrostatic Potential Map. *Biophys. J.* **2005**, *88*, 3745–3761.

(20) Kesselheim, S.; Müller, W.; Holm, C. Origin of Current Blockades in Nanopore Translocation Experiments. *Phys. Rev. Lett.* **2014**, *112*, 018101.

(21) Kowalczyk, S. W.; Wells, D. B.; Aksimentiev, A.; Dekker, C. Slowing Down DNA Translocation through a Nanopore in Lithium Chloride. *Nano Lett.* **2012**, *12*, 1038–1044.